Journal of Clinical and Translational Hepatology **2024** vol. 12(5) | 481–495
DOI: 10.14218/JCTH.2024.00024

Original Article

Astragalus Polysaccharide Enhances Voriconazole Metabolism under Inflammatory Conditions through the Gut Microbiota

Xiaokang Wang[1,2,3#], Xianjing Hu[2,4#], Chunxiao Ye[5], Jingqian Zhao[6], Shing Cheng Tan[7], Liangbin Zhou[8], Chenyu Zhao[6], Kit Hang Wu[9], Xixiao Yang[6], Jinbin Wei[10*] and Maoxun Yang[1,2,4*]

[1]The Marine Biomedical Research Institute of Guangdong Zhanjiang, Zhanjiang, Guangdong, China; [2]Guangdong Provincial Key Laboratory of Research and Development of Natural Drugs, Guangdong Medical University, Dongguan, Guangdong, China; [3]Department of Pharmacy, Shenzhen Longhua District Central Hospital, Shenzhen, Guangdong, China; [4]Dongguan Key Laboratory of Chronic Inflammatory Diseases, The First Dongguan Affiliated Hospital, Guangdong Medical University, Dongguan, Guangdong, China; [5]Department of Pharmacy, The Second Affiliated Hospital of Guangzhou Medical University, Guangzhou, Guangdong, China; [6]Department of Pharmacy, Shenzhen Hospital of Southern Medical University, Shenzhen, Guangdong, China; [7]UKM Medical Molecular Biology Institute, Universiti Kebangsaan Malaysia, Kuala Lumpur, Malaysia; [8]Department of Biomedical Engineering, Faculty of Engineering, The Chinese University of Hong Kong, Hong Kong SAR, China; [9]Department of Pharmacy, Nossa Senhora do Carmo-Lago Health Centre, Health Bureau, Macau, China; [10]Pharmaceutical College, Guangxi Medical University, Nanning, Guangxi, China

Received: 17 January 2024 | **Revised:** 3 April 2024 | **Accepted:** 8 April 2024 | **Published online:** 19 April 2024

Abstract

Background and Aims: Voriconazole (VRC), a widely used antifungal drug, often causes hepatotoxicity, which presents a significant clinical challenge. Previous studies demonstrated that *Astragalus* polysaccharide (APS) can regulate VRC metabolism, thereby potentially mitigating its hepatotoxic effects. In this study, we aimed to explore the mechanism by which APS regulates VRC metabolism. ***Methods:*** First, we assessed the association of abnormal VRC metabolism with hepatotoxicity using the Roussel Uclaf Causality Assessment Method scale. Second, we conducted a series of basic experiments to verify the promotive effect of APS on VRC metabolism. Various *in vitro* and *in vivo* assays, including cytokine profiling, immunohistochemistry, quantitative polymerase chain reaction, metabolite analysis, and drug concentration measurements, were performed using a lipopolysaccharide-induced rat inflammation model. Finally, experiments such as intestinal biodiversity analysis, intestinal clearance assessments, and *Bifidobacterium bifidum* replenishment were performed to examine the ability of *B. bifidum* to regulate the expression of the VRC-metabolizing enzyme CYP2C19 through the gut–liver axis. ***Results:*** The results indicated that APS does not have a direct effect on hepatocytes. However, the assessment of gut microbiota function revealed that APS significantly increases the abundance of *B. bifidum*, which could lead to an anti-inflammatory response in the liver and indirectly enhance VRC metabolism. The dual-luciferase reporter gene assay revealed that APS can hinder the secretion of pro-inflammatory mediators and reduce the inhibitory effect on *CYP2C19* transcription through the nuclear factor-κB signaling pathway. ***Conclusions:*** The study offers valuable insights into the mechanism by which APS alleviates VRC-induced liver damage, highlighting its immunomodulatory influence on hepatic tissues and its indirect regulatory control of VRC-metabolizing enzymes within hepatocytes.

Citation of this article: Wang X, Hu X, Ye C, Zhao J, Tan SC, Zhou L, *et al*. *Astragalus* Polysaccharide Enhances Voriconazole Metabolism under Inflammatory Conditions through the Gut Microbiota. J Clin Transl Hepatol 2024;12(5):481–495. doi: 10.14218/JCTH.2024.00024.

Keywords: *Astragalus* polysaccharide; Voriconazole; Metabolism; RUCAM; *Bifidobacterium bifidum*; Anti-inflammatory responses; Gut Microbiota; Hepatotoxicity.

Abbreviations: APS, *Astragalus* polysaccharide; *B. bifidum*, *Bifidobacterium bifidum*; CYP2C19, Cytochrome P450 2C19; CYP3A4, Cytochrome P450 3A4; HE, hematoxylin-eosin; LPS, lipopolysaccharide; NF-κB, Nuclear factor-κB; PICRUSt, Phylogenetic Investigation of Communities by Reconstruction of Unobserved States; RUCAM, Roussel Uclaf Causality Assessment Method; VRC, voriconazole.

[#]Contributed equally to this work.

[*]**Correspondence to**: Maoxun Yang, Guangdong Provincial Key Laboratory of Research and Development of Natural Drugs, and School of Pharmacy, Guangdong Medical University, No.1, Xincheng Road, Dongguan, Guangdong 523808, China. ORCID: https://orcid.org/0000-0003-0016-039X. Tel: +86-769-22896599, Fax: +86-769-22896560, E-mail: yangmaoxun@gdmu.edu.cn; Jinbin Wei, Pharmaceutical College, Guangxi Medical University, Nanning, Guangxi 530021, China. ORCID: https://orcid.org/0000-0002-6813-6428. Tel/Fax: +86-771-5358562, E-mail: wjbguangxi@sina.cn

Introduction

Currently, the number of patients with fungal infections or immunodeficiency is increasing globally.[1,2] Consequently, the antifungal agent voriconazole (VRC) is being used with increasing frequency. Nevertheless, patients are experiencing complications because of its toxic and adverse effects. Clinical investigations have revealed that VRC metabolism exhibits significant interindividual variability, primarily because

of differences in the activity of hepatic drug-metabolizing enzymes in patients with inflammatory disorders.[3] Consequently, this variability leads to drug-induced hepatotoxicity and the development of optic nerve dysfunction.[4] Analyses of intestinal 16S/ITS and metagenomics revealed notable disparities in the composition and functionality of the intestinal microbiota between populations exhibiting these variations.[5] In the context of acute myeloid leukemia, patients often experience impaired immune function and systemic infections.[6,7] Hence, investigating alterations in both the structure and function of the intestinal microbiota associated with inflammatory conditions could provide insights into the modifications of hepatic drug metabolism.[8] Polysaccharides from traditional Chinese medicine, which serve as prebiotics, modulate the composition of the intestinal microbiota or utilize the fermentation byproducts of the intestinal microbiota to achieve favorable therapeutic outcomes in the management of various conditions, such as diet-induced obesity, colitis, and antibiotic-associated diarrhea.[9]

Polysaccharide preparations can regulate the body's immunity via the gut–liver axis.[10] Furthermore, these preparations have displayed potential to alleviate inflammatory diseases, including non-alcoholic fatty liver disease.[11,12] Astragalus membranaceus, a traditional Chinese medicine, is derived from the dried root of the perennial leguminous plant *Astragalus membranaceus* (Fisch.) Bge. var. mongholicus (Bge.) Hsiao or *A.* membranaceus (Fisch.) Bge.[13] This medicinal herb is characterized by its slightly warm nature and sweet taste, and it is known for its therapeutic properties such as nourishing qi, raising yang, fixing the surface, and stopping sweating. *Astragalus* polysaccharide (APS), one of the main active ingredients of *Astragalus*, can boost immunity, strengthen the heart, protect the liver, reduce blood pressure and diuresis, slow aging, and prevent free radical damage.[14] Injectable APS is extensively used in clinical practice in China, especially for patients receiving chemotherapy, and favorable outcomes have been recorded.[15] Numerous prescription studies illustrated that APS can modulate gastrointestinal motility, counteract gastrointestinal mucosal damage, regulate intestinal immunity, and mitigate the effects of chemotherapeutic agents on the intestinal flora.[13,16,17] However, the effect of APS on liver drug metabolism in disease states has not been reported.

Pharmacokinetics encompasses the examination of drug movement within the human body through absorption, distribution, metabolism, and excretion. The liver is the primary organ responsible for drug metabolism. A crucial mechanism of drug metabolism within the liver involves the cytochrome P450 superfamily (CYPs) of membrane-bound hemoprotein isoenzymes. CYPs comprise the major phase I oxidation systems, and their function is closely linked to systemic drug exposure. CYP2C19 plays a pivotal role in catalyzing the metabolism of various xenobiotics and endobiotics, including VRC and omeprazole. CYP2C19 is abundantly expressed in the rat liver and is readily affected by inflammation, which impairs the ability of the enzyme to metabolize its substrates.

The nuclear factor-κB (NF-κB) pathway is a well-established and crucial signaling mechanism involved in inflammation, and it is primarily activated by pro-inflammatory cytokines such as interleukin l (IL-1) and tumor necrosis factor α (TNF-α). Following lipopolysaccharide (LPS)-triggered inflammation, pro-inflammatory cytokine production in the liver is enhanced. NF-κB consists of the subunits p50 and p65, which combine to form a heterodimer. In the regulation of target genes, NF-κB can act as a transcriptional activator or repressor by interacting with various co-regulatory proteins, including co-activators and co-repressors. NF-κB can regulate the expression and activity of CYPs (*e.g.*, CYP3A) at the transcriptional or post-transcriptional level.[18]

The objectives of our study were to investigate the pharmacokinetic impact of APS on VRC and elucidate the specific mechanism by which APS regulates VRC metabolism. To achieve this aim, we developed a rodent LPS-induced liver inflammation model and subsequently performed pharmacokinetic experiments of VRC in APS-treated and control rats. CYP2C19, an important metabolic enzyme responsible for the elimination of VRC N-oxide, was detected in the livers of rats with inflammation. Furthermore, we investigated the potential effects of the inflammatory microenvironment in the liver on the NF-κB signaling pathway and CYP2C19 transcription. This research aimed to provide targeted prevention and treatment strategies to reduce the incidence of VRC-induced toxicity in patients with underlying medical conditions.

Methods

Acquisition of published cases of VRC-induced hepatotoxicity

Initially, we searched for cases of VRC-induced hepatotoxicity using PubMed, including clinical data, and assessed the findings using the updated Roussel Uclaf Causality Assessment Method (RUCAM) to verify causality. Subsequently, we conducted basic research to explore the ability of APS to prevent and treat VRC-induced hepatotoxicity to provide an early scientific basis for clinical treatment.

Animals and drug treatment

Specific pathogen-free (SPF) Sprague-Dawley rats (male, 6 weeks old, weighing 200–220 g) were obtained from the Laboratory Animal Center of Nanfang Hospital, Southern Medical University (Medical Experimental Animal Number: SCXK-2016-0041). Rats were housed under a 12-h/12-h light/dark cycle at 25±2°C and 55±10% humidity. All rats were acclimatized for 1 week prior to the experiment. At 24 h after VRC administration, the animals were euthanized, their intestinal tracts and intestinal feces were separated, and immunoblotting and 16S rRNA sequencing were performed.

Rats were treated with a single dose of phosphate-buffered saline (PBS) or LPS (0.1 mg/kg suspended in PBS) and subsequently killed by cervical dislocation to obtain liver tissue and peripheral blood. Blood was collected and stored in a refrigerator at −20°C. The expression of inflammatory factors in the liver and the levels of liver tests (LTs) were determined at 2 and 16 h after LPS treatment, respectively. Untreated rats and sterile rats (*i.e.*, rats that had been treated with antibiotics for 4 weeks) were treated with LPS, and then liver inflammatory factor and serum alanine aminotransferase (ALT) levels were measured.

After a 1-week acclimatization period, all rats were randomly divided into four groups (10 rats/group): normal group (Ctrl), model group (LPS), LPS + low-dose APS group (APSL), and LPS + high-dose APS group (APSH). The rats in the Ctrl and LPS groups received 0.5% sodium carboxymethylcellulose solution (CMC-Na) orally. After 1 h, the animals received a second dose of 10 mL/kg CMC-Na orally. Rats in the APSL and APSH groups received APS (suspended in 0.5% CMC-Na) intragastrically at 300 and 600 mg/kg body weight, respectively. The results were recorded every 3 days. The perfusion volume was based on the rats' body weight. The entire animal experiment lasted 4 weeks. A schematic representation of the experimental procedure is presented in Figure 1A. After the experiment, the rats were weighed and fasted for 12 h with free access to water. Blood samples

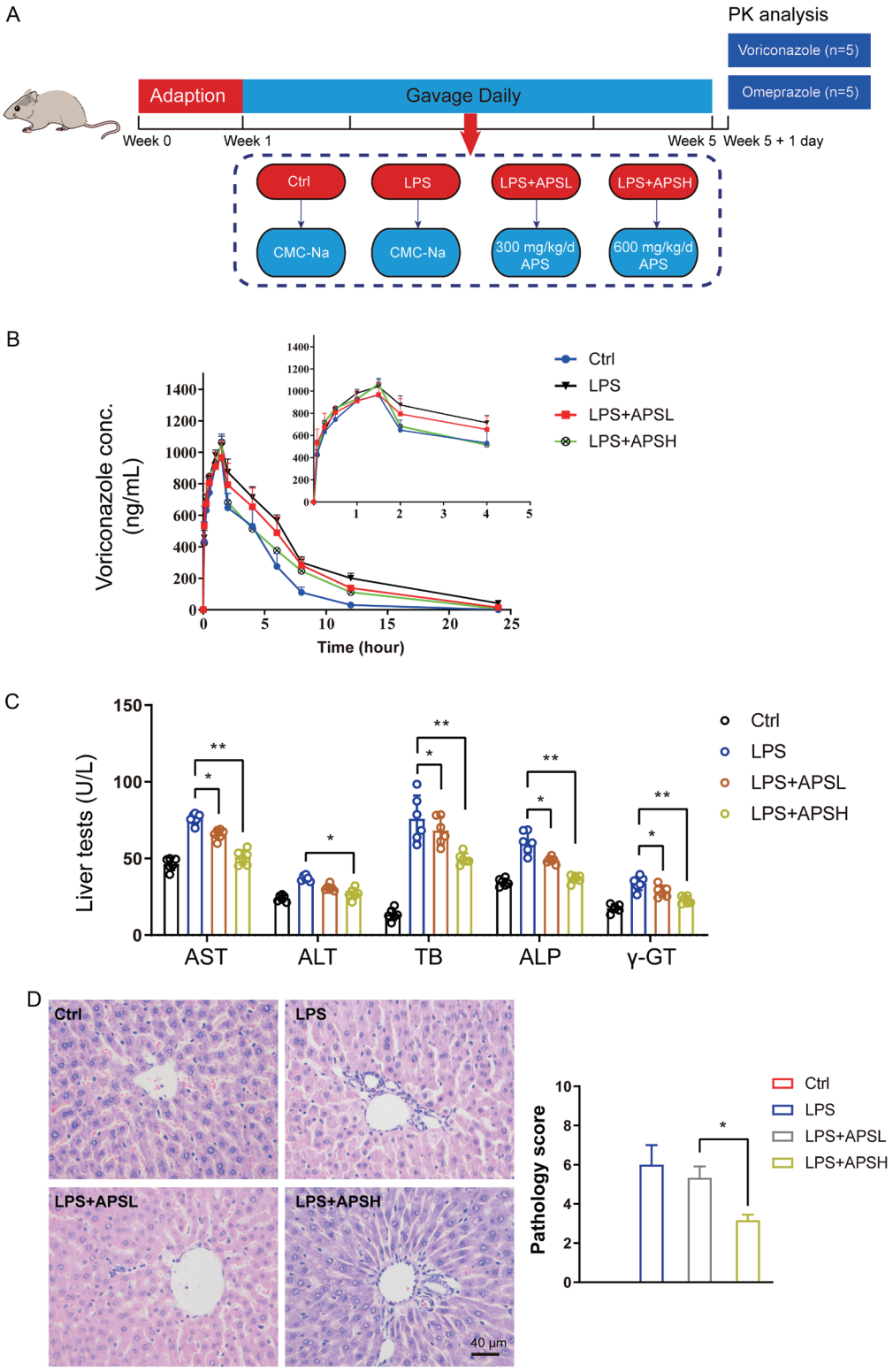

Fig. 1. APS reduces liver inflammation and promotes the metabolism of voriconazole *in vivo*. (A) Schematic diagram of the current experimental process. (B) VRC plasma kinetics in individual rats (n=5, respectively). (C) Effects of APS on LPS-induced inflammatory rat liver tests (LTs). Data are expressed as mean±SD (n=6). (D) Liver pathology score. Left, H&E of liver tissue in each group; Right, Statistical analysis of pathology scores; Bar = 40 μm. Data are expressed as mean±SD (n=3). $^{**}P<0.01$, $^{*}P<0.05$ *vs.* LPS group. ALP, Alkaline phosphatase; ALT, Alanine aminotransferase; APS, *Astragalus* polysaccharide; APSH, high-dose APS group; APSL, low-dose APS group; AST, Aspartate aminotransferase; Ctrl, Control group; H&E, Hematoxylin-eosin staining; LPS, lipopolysaccharide; SD, standard deviation; TB, Total bilirubin; TG, Triglycerides; VRC, Voriconazole; γ-GT (GGT), γ-glutamyl transferase.

were collected from the orbital venous plexus of the rats and stored at 4°C for 12 h. After blood collection for the pharmacokinetic experiment, the animals in each group were anesthetized with chloral hydrate, rinsed with 50 mL of physiological saline in a pre-cooler, and then collected for later use. After sacrifice, organ tissues were removed, and the liver samples were divided into two parts. One part was placed in 10% formalin solution for histopathological examination and homogenization, and the other part was stored at −80°C for biochemical assays. The contents of the colon were collected and stored at −80°C for gut microbiota analysis.

Bifidobacterium bifidum was obtained from the Center of Industrial Culture and the BeNa Culture Collection of China. After resuscitation, *B. bifidum* was cultured in chocolate-colored blood medium or BBL liquid medium. For both media, the strain was incubated at 37°C on an anaerobic table, centrifuged at 4°C for 5 min at 18,000 ×*g*, and washed twice with sterile PBS to prepare a bacterial solution with a concentration of 1×10^9 CFU/mL for use in the next step.

Treatment with an antibiotic cocktail

After a 1-week acclimatization period, SPF rats were administered an antibiotic cocktail (1 g/L streptomycin, 0.5 g/L ampicillin, 1 g/L gentamicin, and 0.5 g/L vancomycin) *via* a nasogastric tube (500 μL/each) three times a week for 2 weeks. The antibiotics were administered in drinking water to avoid confounding effects attributable to the stress induced by oral gavage. At the end of bacterial clearance, quantitative reverse transcription-polymerase chain reaction (qRT-PCR) was performed to determine the total bacterial count in feces. All antibiotics were purchased from Meilun Bio (Dalian, China).

Reagents

LPS was acquired from MCE (Monmouth Junction, NJ, USA). A primary antibody against multidrug resistance gene 1 (P-gp) was purchased from Cell Signaling Technology (Danvers, MA, USA). Other antibodies were purchased from Invitrogen (Carlsbad, CA, USA). Background fluorescence was determined using an anti-rat isotype control antibody (BD Pharmingen, Franklin Lakes, NJ, USA).

16S rRNA-sequencing analysis

To ensure the successful establishment of the rodent model of intestinal dysbacteriosis and to understand the difference in intestinal dysbacteriosis between the two groups, fecal samples were collected 8 days after ceftriaxone sodium or sterile water administration.

Microbial community genomic DNA was extracted from fecal samples using the E.Z.N.A.® DNA kit (Omega Bio-tek, Norcross, GA, U.S.) according to the manufacturer's instructions. One percent agarose gel electrophoresis was performed to determine the quality of DNA, and NanoDrop 2000 (Thermo Scientific, Waltham, MA, USA) was used to determine the concentration and purity of DNA. The V3–V4 hypervariable region of the 16S rRNA gene was amplified by PCR using the primers 338F (5′-ACTCCTACGGGAGGCAGCAG-3′) and 806R (5′-GGACTACHVGGGTWTCTAAT-3′). After amplification, 2% agarose gel electrophoresis was used to recover the PCR products. Then, the obtained products were purified using an AxyPrep DNA Gel Extraction Kit (Axygen Biosciences, Union City, CA, USA) and quantified using a Quantus Gel Fluorometer (Promega, Madison, WI, USA). NEXTFLEX Rapid DNA-Seq kits (BioScientific, Austin, TX, USA) were used for paired-end library construction. Paired-end sequencing was performed with Illumina MiSeq PE300/NovaSeq PE250 (Illumina Inc., San Diego, CA, USA) using standard protocols at Majorbio Bio-Pharm Technology Co. Ltd. (Shanghai, China). The data analysis pipeline, including correlation analysis of environmental factors and selected species or OTUs, was generated using Majorbio Biomedical Technology's cloud platform, which provided an intuitive heatmap representation of the numerical matrix derived from the correlation analysis. In addition, Phylogenetic Investigation of Communities by Reconstruction of Unobserved States (PICRUSt) was employed to predict the metabolic functions of bacterial communities and the functional composition of metagenomes. The PICRUSt analysis involved normalizing the COG information and the KEGG Orthology (KO) information for each ID gene. The abundance of each KO and COG was then calculated to obtain the corresponding functional abundance spectrum using data from the COG and KEGG databases. The analysis divided the functional categories into different pathway levels, permitting a detailed examination of the functions of the bacterial community at different biological hierarchy levels.

Pharmacokinetic analysis

All rats in the inflammatory response model group were injected with 100 μg/kg LPS through the tail vein. Blood was collected at 0, 0.08, 0.25, 0.5, 1, 1.5, 2.0, 4.0, 6.0, 8.0, 12.0, and 24.0 h after a single dose of VRC (20 mg/kg) into heparin-containing tubes with anticoagulant, and plasma was obtained by centrifuging the blood at 13,000 rpm for 10 min and collecting the supernatant. The VRC concentration was determined by high-performance liquid chromatography (HPLC)-tandem mass spectrometry (MS/MS). All samples were centrifuged at 3,500 rpm at 4°C for 15 min. The supernatant (plasma) was removed and stored at −80°C. During the analysis, the plasma (50 μL) was mixed with acetonitrile (200 μL) to precipitate the proteins. After high-speed centrifugation (13,000 rpm, 10 min), the transparent supernatant was collected, evaporated with flowing N_2 gas, redissolved in 100 μL acetonitrile/0.1% formic acid (40/60, v/v), and analyzed by HPLC using standard solutions and quality control. The PK Solver software program was used for data analysis.

HPLC-MS/MS conditions

The concentrations of VRC and omeprazole were determined using a Waters ACQUITY UPLC- QTOF system (Waters, Milford, MA, USA). An ACQUITY UPLC BEH C18 1.7 μm column (Waters) was used at a temperature of 40°C. Chromatographic separation was achieved using a gradient mobile phase consisting of 0.01% formic acid in water (A) and acetonitrile (B) at a flow rate of 0.3 mL/min as follows: VRC, 5–99% B (0–5.0 min); 99% B (5.0–7.0 min); 99–5% B (7.0–7.1 min); 5% B (7.1–10.0 min); omeprazole, 10–85% B (0–1.5 min); 85% B (1.5–6.0 min); 85–10% B (6.0–7.0 min), and 10% B (7.0–10.0 min). The analytes were quantified by electrospray ionization in the MS scan mode. Detail method of VRC and N-oxide UPLC-MS/MS analysis can refer to the Supplementary File 1.

Determination of biochemical indicators in serum and the liver

Blood samples were centrifuged at 4,000 ×*g* for 15 min at 4°C to collect the serum. According to the instructions of the corresponding kit, a Mindray BS-420 automatic biochemical analyzer (Shenzhen Minde Biomedical Electronics Co., Ltd., Shenzhen, China) was used to detect biochemical indicators such as triglycerides (TGs), total cholesterol (TC), free fatty acids (FFAs), high-density lipoprotein, low-density lipoprotein, aspartate AST, ALT, total bilirubin (TB), alkaline phosphatase (ALP), and γ-glutamyl transpeptidase (γ-GT). The levels of TG, TC, and FFA in liver homogenate were meas-

Table 1. A list of primer sequences specific to each gene used in qRT–PCR

Gene symbol	Species	Forward primer (5′→3′)	Reverse primer (5′→3′)
16S (338F_806R)	Bacteria	ACTCCTACGGGAGGCAGCAG	GGACTACHVGGGTWTCTAAT
CYP3A4	Rat	TGTATGAACTGGCCACTCACC	TAGCTTGGAATCATCACCACC
CYP2C9	Rat	ACGCGTCCCCATGAACAAAC	AGATCTGGAACAATGCCATG
CYP2C19	Rat	AAATTGTTTCCAATCATTTAGCT	ACTTCAGGGCTTGGTCAATA
IL-6	Rat	AGCTTCCTTGTGCAAGTGTCT	GACAGCCCAGGTCAAAGGTT
IL-1β	Rat	AGGCTGACAGACCCCAAAAG	CTCCACGGGCAAGACATAGG
IL10	Rat	ACTGGCATGAGGATCAGCAG	AGAAATCGATGACAGCGCCT
TNF-α	Rat	AAATGGGCTCCCTCTCATCAGTTC	TCTGCTTGGTGGTTTGCTACGAC
FXR	Rat	CTGTGTGTTGTTTGTGGAGACAGA	ACAGCGTTTTTGGTAATGCTTCT
PXR	Rat	CATCTCAGCAACCCACACAG	GGGGTCATAGGAGTCATTGG
AhR	Rat	TCCCTTATGAGTGCCTTGA	GTCTGATTTCCTCGTGTTTC
GAPDH	human	GTCTCCTCTGACTTCAACAGCG	ACCACCCTGTTGCTGTAGCCAA
GAPDH	Rat	GCAAATTCCATGGCACCGT	TCGCCCCACTTGATTTTGG

16S (338F_806R), 16S rRNA gene V3-V4 region (338F/806R); CYP, Cytochrome P450; IL, Interleukin; TNF, Tumor necrosis factor; FXR, Farnesoid X receptor; PXR, pregnenolone X receptor; AhR, Aryl hydrocarbon receptor.

ured using corresponding detection kits based on liver lipid extraction. Based on the instructions of the respective detection kits, glutathione (GSH), and GSH peroxidase (GSH-Px) activities in the liver were determined. Corresponding ELISA kits were used to detect the levels of inflammatory cytokines (TNF-α, IL-6, and IL-1β). The total liver protein concentration was measured using a BCA kit, and the results were consistent with the liver protein concentration.

Liver pathology score

Following euthanasia, liver tissues were collected from control and experimental rats, fixed with formaldehyde, embedded in paraffin, and sectioned. The sections were stained with hematoxylin and eosin (H&E). The sections were observed under a microscope at ×400 magnification.

Cell culture and treatments

HepG2 and LO2 human hepatocytes were purchased from the Clinical Research Center of Nanfang Hospital. Cells were cultured in DMEM containing 10% fetal bovine serum, 100 U/mL penicillin, and 100 μg/mL streptomycin at 37°C in a 5% CO_2 atmosphere with or without LPS, APS pretreatment, medium replacement, or trypsin digestion. Cells were passaged at a ratio of 1:3 or 1:4 every 2–3 days.

Cell Counting Kit 8 (CCK8) assay

The CCK8 assay (Boster, Wuhan, China) was conducted using HepG2 and LO2 cells to assess the impact of different concentrations of LPS and APS on viability. Furthermore, the appropriate concentration of APS was determined for further investigation of its mechanism of action in HepG2 and LO2 cells. HepG2 and LO2 cells were incubated with different concentrations of LPS (0, 0.01, 0.1, 1, 10 μg/mL) and APS (0, 25, 50, 100, 200, 400, 600 μg/mL) for 24 h. The cells were first washed with PBS. A defined number (200 μL or 1×10^4) of cells was centrifuged after collection and resuspended in fresh medium, and then 10 μL of CCK8 reagent was added to each well of the 96-well plate. The plates were incubated at 37°C for 1.5 h. The control well contained medium and CCK8 reagent with no cells. The absorbance at 490 nm was measured after 0, 24, and 48 h using an ELISA plate reader (Biotek, Winooski, VT, USA). Cell viability was calculated using the following formula:

$$\text{Cell viability (\%)} = \frac{\text{OD (sample)} - \text{OD (blank)}}{\text{OD (control)} - \text{OD (blank)}} \times 100\%.$$

qRT-PCR

The expression of *CYP2C19*, *CYP3A4*, *CYP2C9*, and genes encoding selected inflammatory cytokines and transcription factors was analyzed by qRT-PCR. Samples were homogenized, and mRNA was extracted using TRIzol reagent (Invitrogen). The mRNA concentration was determined using an ABI Prism 7900 Sequence Detection System (Applied Biosystems, Foster City, CA, USA). Total mRNA was dissolved in a 20-mL reaction system, and the RNA was reverse-transcribed to generate cDNA. The reaction system consisted of 1 μL of oligonucleotide (dT) primer, 4 μL of 5× reaction buffer, 1 μL of RNase inhibitor, 2 μL of dNTPs (10 mmol/L), and 1 μL of RT buffer. The mixture was denatured at 42°C for 60 min and annealed at 70°C for 5 min. After RT, 4 mL of each cDNA were dissolved in 50 mL of a PCR mixture consisting of 26 mL of 1×SYBR Green master mix, 1 μL of each primer, and 18 mL of sterile water. The primer sequences for the target genes and the internal control gene glyceraldehyde 3-phosphate dehydrogenase (*GAPDH*) are listed in Table 1. The amplification conditions consisted of initial denaturation at 95°C for 30 s, followed by 60 cycles of 72°C for 5 s and 60°C for 35 s. Fluorescence data were acquired and analyzed at the end of the elongation step in each cycle using ABI 7500 System SDS software version 1.4 (Applied Biosystems). Quantification was performed using the $2^{-\Delta\Delta Ct}$ method based on three replicates to determine the fold change in relative abundance normalized to endogenous *GAPDH* expression.

Dual-luciferase reporter gene assay

The plasmid pGL3-CYP2C19-luc was used to analyze CYP2C19 activity. The pRL-TK *Renilla* luciferase plasmid (Promega) was used to control transfection efficiency. For the dual-luciferase reporter gene assay, hepatocytes were cultured in 10-cm cell culture dishes at a density of 70–80%. In total, 0.5 μg of pGL3-CYP2C19-luc plasmid or an equivalent amount of con-

Table 2. Published VRC hepatotoxicity cases assessed for causality using RUCAM

Author	Number of hepatotoxicity patients	Number of patients taking VRC	Incidence of VRC hepatotoxicity
Kong *et al*[20]	24	1,798	1.33%
Shen *et al*[21]	18	140	12.9%
Hamada *et al*[22]	24	401	6%
den Hollander *et al*[23]	3	46	6.5%
Cadena *et al*[24]	12	35	34.3%
Zhou *et al*[25]	955	3,245	29.43%

VRC, voriconazole; RUCAM, Roussel Uclaf Causality Assessment Method.

trol plasmid was transfected with Lipofectamine™ 3000 transfection reagent (Invitrogen) according to the manufacturer's protocol. At 24 h post-transfection, cells were treated with or without p65 (200 or 400 ng), and firefly and *Renilla* luciferase reporter signals were immediately determined using the Dual-Luciferase Reporter Gene Assay System (Promega).[19]

Western blotting

All animals were sacrificed to obtain liver tissues. Hepatocytes (1×10^6 cells/well) were plated in six-well plates and incubated in a 5% CO_2 incubator at 37°C overnight. Cells were then treated with lysis buffer containing protease and phosphatase inhibitors (Beyotime Institute of Biotechnology, Nantong, China) for 60 min and centrifuged at 12,000 ×*g* at 4°C for 10 min. The cytosolic and nuclear fractions were prepared using a Nuclear Extract Kit (Active Motif, Carlsbad, CA, USA). The liver of each animal was washed with stroke-physiological saline solution and then homogenized with 1% protease inhibitor in RIPA buffer. After centrifugation (12,000 rpm, 12 min, 4°C), the supernatant was collected for subsequent experiments. The protein concentration was measured using BCA kits. Ten micrograms of total protein lysate were electrophoresed in a 10% SDS-polyacrylamide gel, and the proteins isolated in the gel were transferred to PVDF membranes (EMD Millipore, Billerica, MA, USA). The membranes were blocked for 2 h at room temperature with a 5% milk-blocking solution. The total protein concentration of the supernatant was determined using a SpectraMax M5 multifunctional enzyme marker (Molecular Devices, Sunnyvale, CA, USA). Proteins were separated by 10% SDS-polyacrylamide gel electrophoresis, transferred to PVDF membranes, and blocked for 1.5 h. PVDF membranes were then washed with Tris-buffered saline containing Tween-20 (TBST) and incubated with primary antibodies against P-gp (1:5,000), CYP2C19 (1:1,000), p-p65 (1:500), and p-IκB (1:1,000) at 4°C overnight. After three washes with TBST, the membranes were incubated with a secondary antibody (1:5,000, Cell Signaling Technology) for 1 h at 25°C and then washed three times with TBST. Images were captured using ImageJ to quantify optical density.[5]

Immunfluorescence

After treatment with APSH alone or in combination with *B. bifidum*, rat livers were resuspended on microscopic cover slides in 35-mm dishes, rinsed with PBS, fixed in 4% formalin (for 10 min), washed three times with PBS, and permeabilized with 0.5% Triton X-100 (in PBS) for 5 min. Then, the cells were blocked with 2% bovine serum albumin (Roche, Basel, Switzerland) for 30 min and fixed with a 4% formaldehyde solution at room temperature. Cells were then incubated overnight at 4°C with a rabbit polyclonal anti-P-gp antibody (1:100, Abcam, Cambridge, UK) and fluorescein isothiocyanate-conjugated Affini-Pure goat anti-rat IgG (1:100; Protein-tech Biotechnology Co., Ltd., Wuhan, China) for 1 h at 37°C. The tissues were observed and photographed using a fluorescence microscope (Olympus BX-51, Olympus, Tokyo, Japan) following DAPI staining (1:1,000 in PBS, Sigma-Aldrich, St. Louis, MO, USA).

Statistical analyses

Experimental data are presented as the mean and standard deviation. The data were analyzed using GraphPad Prism 8.0 (GraphPad, La Jolla, CA, USA). Student's *t*-test was used to compare differences between two groups, and differences among multiple groups were assessed using the Kruskal–Wallis test and Dunn *post-hoc* test. Other statistical methods were indicated accordingly. $P<0.05$ denoted statistical significance.

Results

Published clinical evaluation of VRC-induced hepatotoxicity using RUCAM

Judging from the analysis of clinical research reports, VRC-induced hepatotoxicity is an extremely common adverse drug reaction. According to the clinical RUCAM evaluation, the incidence of liver toxicity ranges from 1.33% to 34.3% (Table 2).[20–25] Hence, identifying strategies to reduce VRC-induced hepatotoxicity has clinical significance.

APS reduces liver inflammation and promotes voriconazole metabolism in vivo

In rodent experiments, we first examined the abnormal metabolism of VRC in inflammatory models, finding that APS administration can improve the *in vivo* metabolism of VRC (Fig. 1B). To investigate the effects of APS on hepatic function in rats with LPS-induced inflammation, various liver markers, including AST, ALT, TB, ALP, and γ-GT, were examined in the sera of rats from the LPS and APS groups. Following LPS induction, the levels of markers were significantly increased compared to those in the Ctrl group ($P<0.01$). Compared to the effects of LPS, the reductions in liver indices, including AST, ALT, TB, ALP, and γ-GT, were larger in the APSH group than in the APSL group. These results suggest that high-dose APS administration might be more effective in ameliorating liver abnormalities induced by LPS (Fig. 1C).

LPS was used to induce liver inflammation, resulting in significant pathological changes. APS administration attenuated these changes, as evidenced by the absence of steatosis, edema, and inflammatory cell infiltration in liver tissue. This observation was supported by the comparison of liver cell structure between the Ctrl and LPS groups (Fig. 1D). Furthermore, the severity of liver lesions was quantitatively

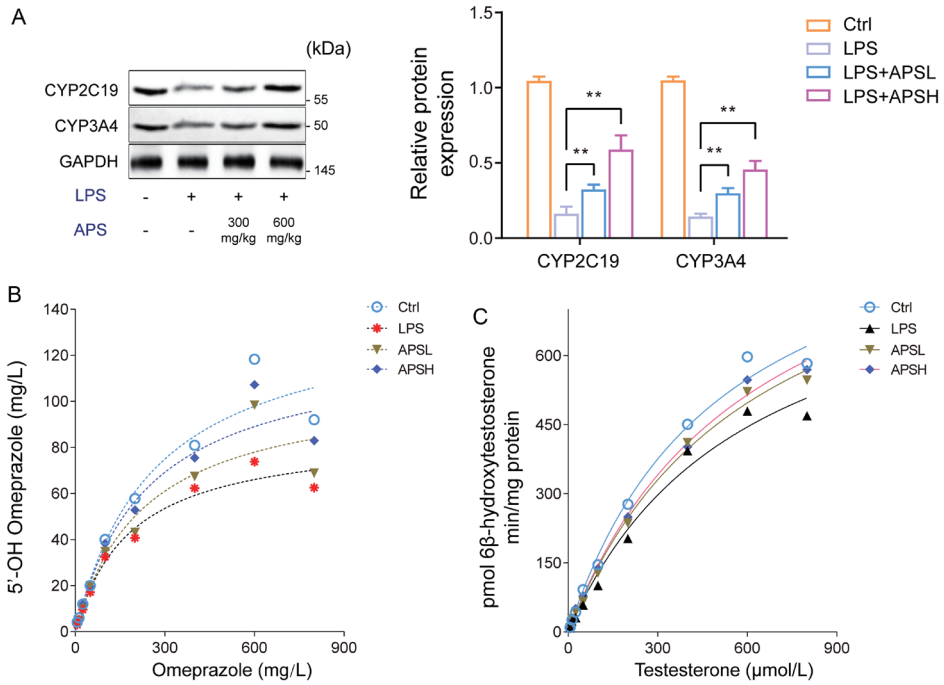

Fig. 2. Effects of APS on CYP2C19 and CYP3A4 enzyme expression *in vivo*. (A) Left, CYP2C19 and CYP3A4 enzyme protein band diagram; Right, CYP2C19 and CYP3A4 enzyme protein statistical analysis histogram in each group. Data represents means±SD (n=3). (B) Determination of CYP2C19 enzyme substrate metabolite concentration; (C) CYP3A4 enzyme substrate metabolite concentration determination. Each point represents means±SD (n=3). ***P*<0.01; +, with; −, without. APS, *Astragalus* polysaccharide; APSH, high-dose APS group; APSL, low-dose APS group; Ctrl, Control group; CYP, Cytochrome P450; LPS, lipopolysaccharide; SD, standard deviation.

assessed, and an average score was assigned to each experimental group. Notably, the liver lobules in the Ctrl group received a score of 0, indicating the absence of any pathological alterations. By contrast, LPS treatment induced obvious liver lesions characterized by liver cord disorder, vesicular steatosis, and significant infiltration of inflammatory cells, resulting in an average liver pathology score of 5.95. However, when low and high doses of APS were administered, the extent of liver damage was reduced, leading to a relatively intact liver cell structure with mild steatosis and limited infiltration of inflammatory cells. Most importantly, high-dose APS administration resulted in the absence of noticeable inflammatory cell infiltration in the pathological tissue.

Effects of APS on CYP2C19 and CYP3A4 activities in vivo

The protein expression of enzymes serves as the basis for their ability to metabolize drugs. Therefore, alterations in functional enzyme expression in liver tissue were assessed by measuring the gene and protein expression of metabolic enzymes. As presented in Figure 2A, CYP2C19 and CYP3A4 protein expression was correlated with APS administration, and a discernible dose-response relationship was observed. This was evidenced by a substantial increase in target protein expression in the APSH group, which was significantly different from that in the LPS group. Thus, APS was demonstrated to promote the activity of specific hepatic enzymes responsible for metabolizing VRC in an inflammatory environment *in vivo*.

Enzymatic activity plays a crucial role in drug metabolism. Details of rat liver microsomes, intestinal microsomes preparation have been descript in the Supplementary File 1. Thus, in this study, we used metabolic enzyme substrates as probes to assess alterations in enzyme activity in liver tissue. As illustrated in Figure 2B, omeprazole, a specific substrate metabolized to 5′-OH-omeprazole by CYP2C19, induced notable changes. In particular, in the LPS group, APS administration significantly increased the production of 5′-OH-omeprazole, suggesting that APS administration effectively increased CYP2C19 activity in the liver. From the results presented in Figure 2C, testosterone is a clear substrate for CYP3A4, and it is metabolically converted to 6β-OH-testosterone by this enzyme. Table 3 illustrates that APS administration significantly

Table 3. Effects of APS on the activities of CYP2C19 and CYP3A4 *in vivo*

Group	5′-OH omeprazole		6β-hydroxytestosterone	
	Km	Vmax	Km	Vmax
Ctrl	265±80.13	141.1±16.79	514.8±71.98	1,020±72.11
LPS	183.9±42.52	86.3±6.897	592.1±81.5	884±88.68
APSL	230.4±80.13	107.9±14.03*	612.2±43.89*	1,004±74.23
APSH	241.3±61.97*	124.8±12.26*	620.3±34.08*	1,046±37.72*

Data are presented in mean±SD (n=3), **P*<0.05. Ctrl, Control group; LPS, Lipopolysaccharide; APSL, LPS + low-dose APS group; APSH, LPS + high-dose APS group; CYP, Cytochrome P450.

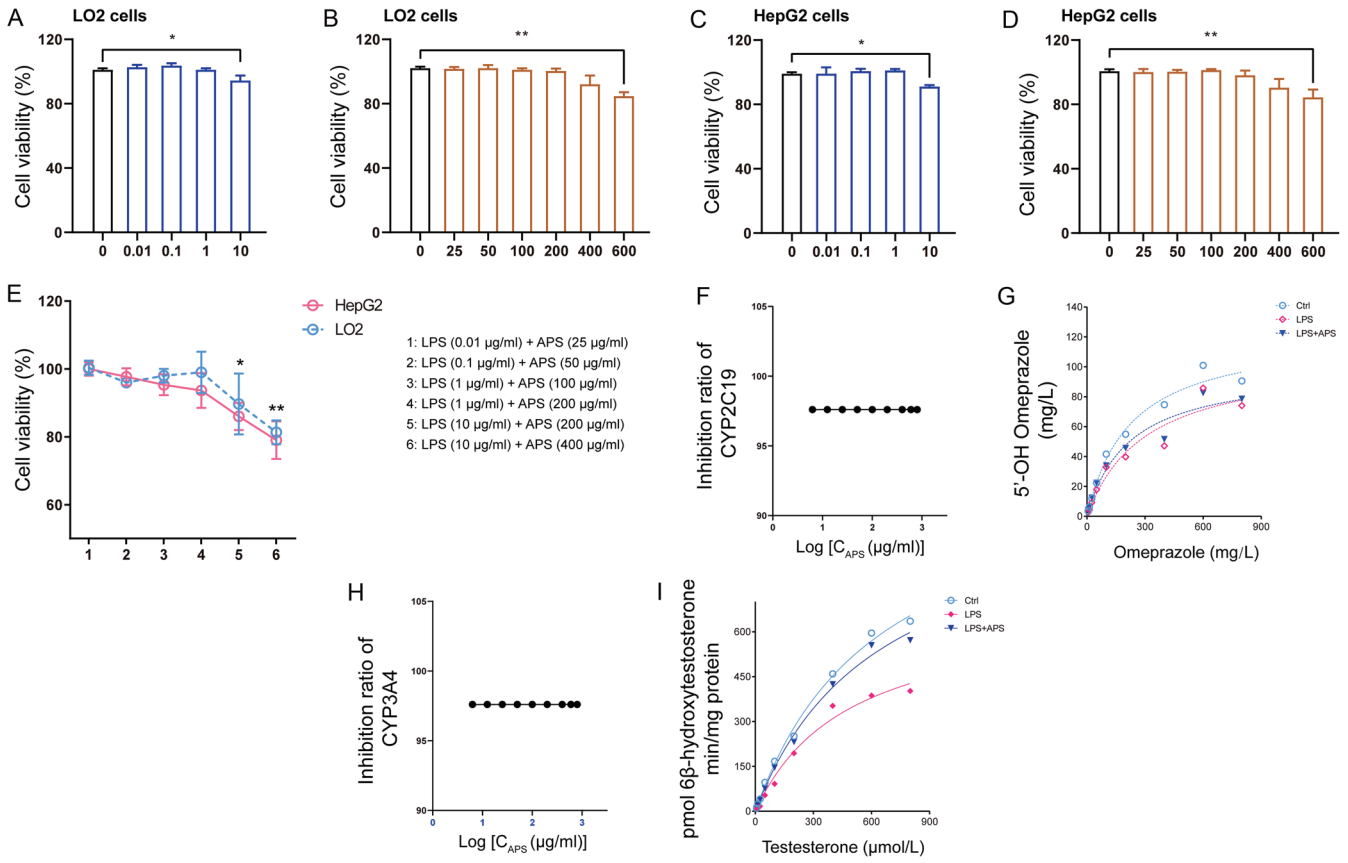

Fig. 3. Effects of LPS and APS on the viability of humanized hepatocytes. (A) the effect of different concentrations of LPS on the activity of LO2 cells; (B) the effect of different concentrations of APS on the activity of LO2 cells; (C) the effect of different concentrations of LPS on the activity of HepG2 cells; (D) the effect of different concentrations of APS on the activity of HepG2 cells Effects on HepG2 cell viability. (E) Effects of different concentrations of LPS+APS on the viability of LO2/HepG2 cells. (F, G) Measurement of CYP2C19 enzyme inhibition and enzyme substrate metabolite concentrations. (H, I) Measurement of CYP3A4 enzyme inhibition and enzyme substrate metabolite concentrations. Data are represented as the means±SD (n=3). $^{**}P<0.01$, $^{*}P<0.05$ compared with the control group, $^{**}P<0.01$, $^{*}P<0.05$. APS, *Astragalus* polysaccharide; C, Concentration; Ctrl, Control; CYP2C19, Cytochrome P450 2C19; CYP3A4, Cytochrome P450 3A4; LPS, lipopolysaccharide; SD, standard deviation.

increased the production of 6β-OH-testosterone. Furthermore, APS induced an increase in hepatic CYP3A4 activity.

Effects of APS on CYP2C19 and CYP3A4 activities in vitro

The ability of LPS and APS to stimulate hepatic enzyme activity was assessed *in vitro* to clarify the mechanisms underlying the observed *in vivo* results. High concentrations of LPS (10 μg/mL, both $P<0.05$) and APS (600 μg/mL, both $P<0.01$) reduced viability in LO2 (Fig. 3A, B) and HepG2 cells (Fig. 3C, D). In addition, the impact of different combinations of LPS and APS concentrations on cell viability was investigated. LPS (1 μg/mL) + APS (100 μg/mL) did not alter viability in either cell line ($P>0.05$, Fig. 3E). Conversely, LPS (10 μg/mL) in combination with higher concentrations of APS (200 and 400 μg/mL) remarkably reduced cell viability ($P<0.05$). Meanwhile, although LPS (1 μg/mL) + APS (200 μg/mL) did not alter the viability of LO2 cells, the combination reduced the viability of HepG2 cells. Considering that LPS can be used to establish a more efficient inflammatory cell model without affecting cell viability, we set the *in vitro* concentration of LPS at 1 μg/mL. These findings were combined to facilitate further investigation of the impact of LPS in conjunction with APS on the activity and expression of CYPs. Consequently, we set the optimal LPS concentration as an inflammatory stimulus in the *in vitro* model at 1 μg/mL, while the concentration of APS was set at 100 μg/mL.

We then used the liver microsomal metabolic system to further investigate the impact of APS on CYP2C19 and CYP3A4 activity *in vitro* (Fig. 3F–I). In the group subjected to LPS-induced inflammation, APS administration did not significantly alter the production of 5′-OH-omeprazole, suggesting that APS administration did not affect CYP2C19 activity in the *in vitro* inflammatory model. Furthermore, APS administration did not influence the production of 6β-OH-testosterone, suggesting that the compound does not directly influence the expression of VRC-metabolizing enzymes in the inflammatory state.

Effects of APS on P-gp transport activity and expression in HepG2 cells

The mRNA expression of VRC-metabolizing enzymes in human hepatocytes was examined **(**Fig. 4A, B**)**. CYP2C19 and CYP3A4 were downregulated after LPS stimulation. Compared to the findings in the Ctrl or LPS group, APS administration did not significantly alter the expression of CYP2C19 and CYP3A4. This suggests that diseases associated with inflammation might result in CYP2C19 and CYP3A4 downregulation, whereas APS does not appear to reverse these changes.

Investigation of the influence of APS on P-gp–mediated VRC transport represented a crucial subsequent phase of this study. For this purpose, HepG2 cells, a commonly used cellu-

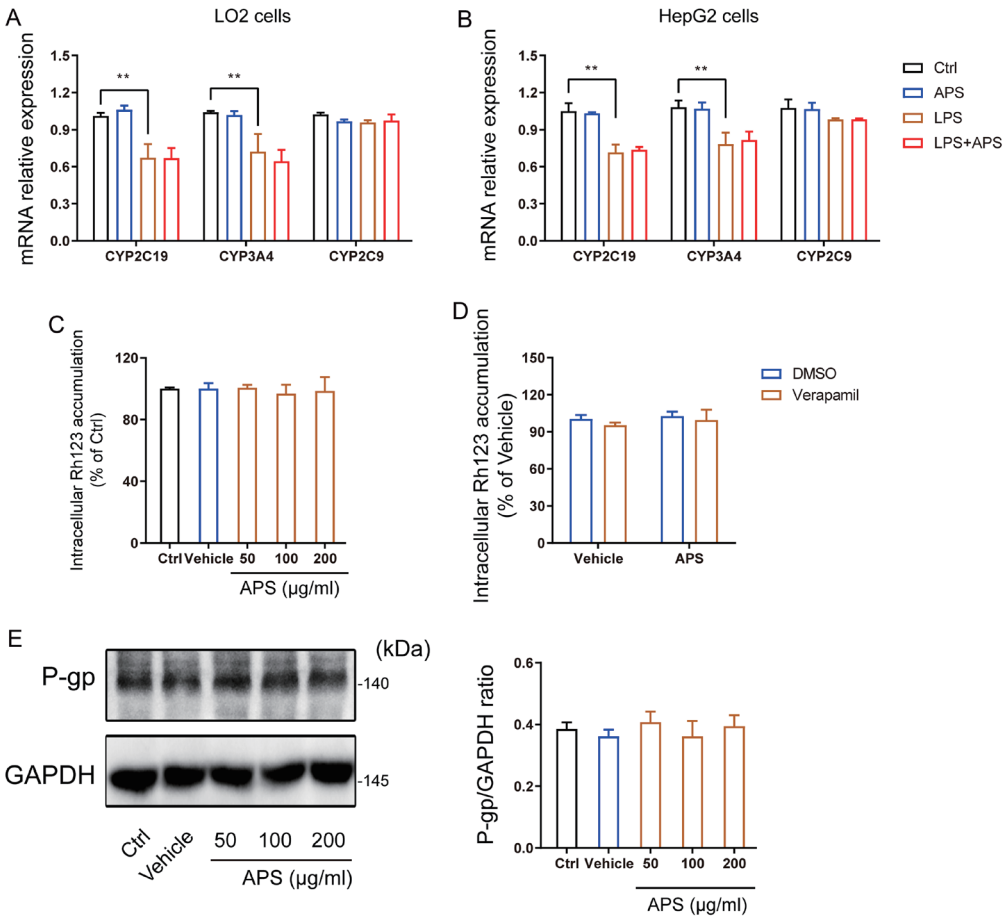

Fig. 4. Effect of LPS and APS on mRNA expression of humanized hepatic cytochrome P450s. (A) Effect of APS on voriconazole metabolism-associated P450 (CYPs) gene expression in LO2 cells; (B) Effect of APS on voriconazole metabolism-associated P450 (CYPs) gene expression in HepG2 cells, (C) Analysis of intracellular fluorescence intensity changes of Rh123, a specific probe substrate of P-gp (coding gene ABCB1), with different concentrations of APS; (D) ABCB1-specific inhibitor Verapamil to APS (100 μg/ml) in cells. Analysis of the change of fluorescence intensity; (E) Effect of different concentrations of APS on the expression of P-gp protein. ** *P*<0.01. APS, *Astragalus* polysaccharide; Ctrl, Control; CYP, Cytochrome P450; DMSO, Dimethyl sulfoxide; GAPDH, glyceraldehyde 3-phosphate dehydrogenase; LPS, lipopolysaccharide; P-gp, P-glycoprotein;; Rh123, Rhodamine 123.

lar model to study hepatic transport, were used together with fluorescent probes and their corresponding inhibitors. As presented in Figure 4C, D, treatment with APS at concentrations of 50, 100, and 200 μg/mL resulted in noticeable modifications of the intracellular fluorescence intensity of the ABCB1-specific probe substrate Rh123. Compared to the findings in the Ctrl group, 100 and 200 μg/mL APS did not reduce the fluorescence intensity of the substrate (P>0.05). The administration of verapamil, a specific inhibitor of ABCB1, also did not affect the induction of P-gp by APS (P>0.05). Additionally, western blotting confirmed that P-gp protein expression was not different following exposure to different concentrations of APS (Fig. 4E). These results indicate that APS does not influence P-gp transport activity in HepG2 cells.

The bacterial strain Bifidobacterium might play a vital role in the regulation of voriconazole metabolism in vivo

Based on the results of the *in vitro* studies illustrating that APS had little direct effect on the expression and activity of the metabolic enzymes associated with VRC, we speculate that APS can regulate VRC metabolism in liver cells through its influence on the intestinal flora and structure, thereby indirectly improving abnormal VRC metabolism in an inflammatory state. To test this hypothesis, we conducted a comparative analysis of the variations in the intestinal flora following APS administration. As presented in Figure 5A, the abundance of *Proteobacteria* was lower in the LPS group than in the Ctrl group. Meanwhile, the abundance of *Firmicutes* was increased and that of *Bifidobacterium* was decreased in the LPS group. Conversely, an increase in the abundance of *Proteobacteria* and a decrease in the abundance of *Firmicutes* were observed in the APS group compared to the LPS group. In addition, the abundance of *Bifidobacterium* increased with the APS dose. Furthermore, we analyzed disparities in shared bacterial species at the family level. Venn diagrams were used to quantify the number of common and unique species in multiple groups or samples to provide a more intuitive visualization of compositional similarities and overlap of species (*e.g.*, OTUs) in different environmental samples. As presented in Figure 5B, 10 bacterial species were shared by the APSH and Ctrl groups, whereas only one bacterial species was shared between the LPS and APSH groups. In addition, the APSL group shared five bacterial species with the Ctrl group, whereas seven bacterial species were shared by the LPS and APSL groups.

To functionally assess the gut microbiota, Spearman's cor-

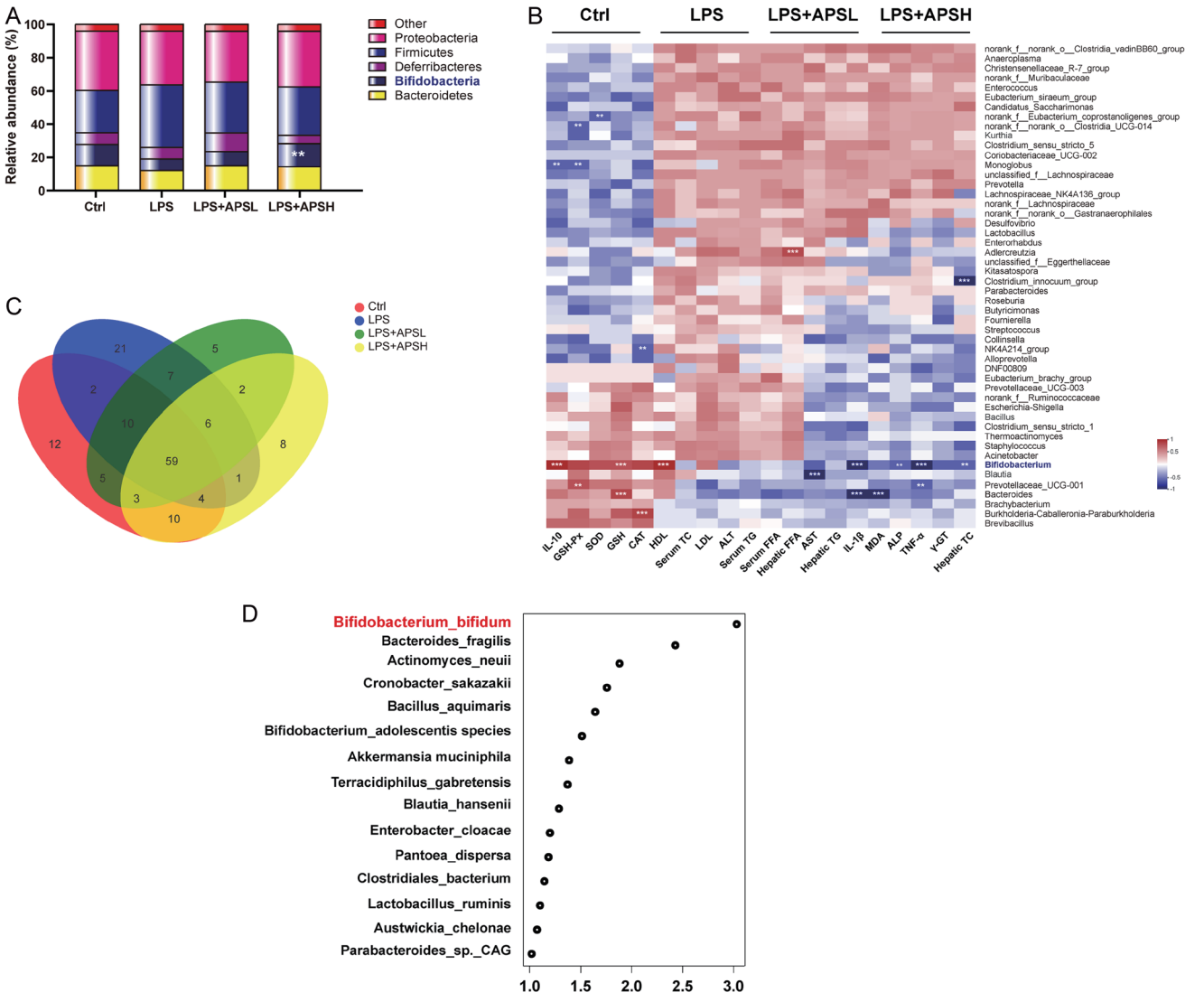

Fig. 5. Effects of APS on the changes of the gut microbiota composition in rats. (A) The relative abundance of bacteria at the phylum level in the gut. (B) Venn diagrams of bacteria at the family level in the gut (n=6). (C) A heatmap showing the relationship between biological parameters and the relative abundance of colonic microbiota at the genus level based on Spearman's correlation analysis. (D) A VIP score of PLS-DA is used to rank the discriminating power of different taxa between the APSH and LPS groups based on their VIP scores. It was determined that a taxon with a VIP score >1 was important for discrimination. $^{**}P<0.01$, $^{***}P<0.001$ APS, *Astragalus* polysaccharide; APSH, high-dose APS group; APSL, low-dose APS group; Ctrl, Control group; LPS, lipopolysaccharide; PLS-DA, partial least squares-discriminant analysis.

relation analysis was performed to examine the relationship between the microbial flora and biochemical indicators (Fig. 5C). The presence of anti-inflammatory or antioxidant factors in serum was positively correlated with the abundance of *Bifidobacterium*. In addition, serum IL-10, GSH, and HDL levels were positively correlated with the abundance of *Bifidobacterium* ($P<0.001$). Furthermore, serum GSH-Px levels displayed a robust positive correlation with the abundance of *Prevotellaceae_UCG-001* ($P<0.001$). Similarly, serum GSH levels were positively correlated with the abundance of both *Bifidobacterium* and *Bacteroides* ($P<0.001$). The serum levels of pro-inflammatory factors (IL-1β and TNF-α) were negatively correlated with the abundance of *Bacteroides* ($P<0.001$). In addition, serum AST and IL-1β levels had strong negative correlations with the abundance of *Bifidobacterium* ($P<0.001$). The analysis of the variable importance in the projection of the gut microbiota illustrated that the contribution of *B. bifidum* differed between the APSH and LPS groups (Fig. 5D).

B. bifidum plays an important role in inhibiting liver inflammatory responses and promoting voriconazole metabolism

To confirm the significant role of *B. bifidum* in the regulation of VRC metabolism by APS, we performed mechanistic analysis using a rat liver inflammation model and a sterile model. The workflow diagram illustrating the experimental procedure is presented in Figure 6A. On the first day following 4 weeks of continuous observation, the pharmacokinetics of VRC were measured in each group of animals. Fresh liver tissue was isolated, and the inflammatory factor levels were determined. After APS administration, inflammatory indicator levels were effectively improved in the livers of rats with LPS-induced inflammation, as presented in Figure 6B–E. Importantly, *B. bifidum* exhibited significant ability to decrease

pro-inflammatory factor levels and increase levels of the anti-inflammatory factor IL-10 in liver secretions in the sterile model group. This indicates that APS can alter inflammatory factor levels in the liver through influencing bacteria. The results of ELISA were further confirmed by a series of inflammatory gene assays. In the LPS-induced inflammatory rat model, APS administration led to significant decreases in the expression of TNF-α, IL-6, IL-1β, and the anti-inflammatory factor IL-10. The gene expression of inflammatory factors after *B. bifidum* administration was consistent with that observed after APSH administration.

An examination of nuclear transcription factors and drug-metabolizing enzyme genes in isolated hepatocytes revealed significant inhibition of FXR, PXR, AhR, CYP2C19, and CYP3A4 in the LPS group. However, after APSH administration, the nuclear transcription factor PXR and CYP2C19, the key enzyme of VRC metabolism, were significantly downregulated. Moreover, their gene expression was significantly increased in the presence of *B. bifidum*. The trend diagram of the kinetics of VRC metabolism is presented in Figure 6O. After the administration of APSH and *B. bifidum*, VRC metabolism was significantly accelerated, and the greatest effect was observed in the APSH group.

The NF-κB signaling pathway is involved in the regulation of CYP2C19 by APSH or B. bifidum administration

To further investigate the mechanism by which *B. bifidum* regulates CYP2C19 activity, the localization of p65, IL-6, and IκB in liver tissue was examined. Immunofluorescence analysis (Fig. 7A) illustrated that the expression of key proteins of the NF-κB signaling pathway was suppressed following the administration of APSH and *B. bifidum*. The examination of hepatocyte proteins revealed significant inhibition of p-IκB and p-p65 in animals treated with APSH and *B. bifidum*. These findings suggest the possible regulation of CYP2C19 enzyme activity by APSH and *B. bifidum*.

Based on the protein expression results, a target prediction for the binding site of p65, a transcription factor that regulates CYP2C19, was performed. Luciferase reporter assays were performed to examine the impact of p65 overexpression on the luciferase activity of CYP2C19. The results revealed the concentration-dependent repression of luciferase activity driven by a 2.1-kb CYP2C19 promoter (−2.0/+0.1 kb) in hepatocytes (Fig. 7C). In addition, *in silico* analysis predicted the presence of a p65 binding site (−1,156/−1,163 bp) in the promoter region of CYP2C19. To further investigate the regulatory effect of NF-κB on CYP2C19 *in vivo*, ChIP analysis was conducted. The results indicated that hepatic p65 is recruited to the binding sites of CYP2C19 in rats treated with antibiotics alone and antibiotics + *B. bifidum*. However, the recruitment of NF-κB to the binding region in the liver of antibiotic-treated rats was more pronounced than in rats treated with antibiotics + *B. bifidum*. However, there was no noticeable difference in NF-κB accumulation in the distal non-binding region, which served as a negative control (Fig. 7D). These results suggest that NF-κB activation in the rat liver specifically leads to the suppression of CYP2C19 transcription, particularly in antibiotic-treated rats. Thus, this study has demonstrated that APS effectively reduces the hepatic secretion of pro-inflammatory factors, attenuates the transcriptional repression of CYP2C19 *via* the NF-κB signaling pathway, and ultimately enhances the metabolism of VRC (Fig. 7E).

Discussion

In this study, we observed changes in the pharmacokinetics of VRC under LPS-induced inflammatory conditions in rats, manifested as an increase in the area under the curve and decreased clearance, which were reversed by APS administration. We confirmed that APS can increase the abundance of *B. bifidum* in the intestines of rats, exert anti-inflammatory effects through the enterohepatic circulation, and enhance the metabolism of VRC mediated by CYP2C19 in the liver. Intestinal clearance and *B. bifidum* strain replenishment experiments in rats revealed that APS regulated the hepatic metabolism of VRC *via* the anti-inflammatory effects of *B. bifidum*. *In vitro* experiments using human cell lines (LO2 and HepG2) demonstrated that APS had no direct effect on the ability of liver cells to metabolize VRC. In terms of mechanism exploration, the hepatic NF-κB signaling pathway is activated during inflammation, attributable to the increased levels of pro-inflammatory cytokines in the liver. Activated NF-κB suppresses CYP2C19 transcription by binding to the NF-κB binding site at −1,720 to −1,711 bp in the promoter. In animals treated with a single *B. bifidum* strain, the bacterium can exert an inhibitory effect on liver inflammation through the enterohepatic axis, reducing the expression of pro-inflammatory factors in the liver, and suppressing the inhibitory effect of inflammatory factors on CYP2C19 transcription. Overall, we found that APS can abrogate LPS-induced CYP2C19 transcriptional inhibition in the liver and promote VRC metabolism in inflammatory disease states *in vivo* by regulating the abundance of *B. bifidum* in the intestine. These results are based on the gut-liver axis, clarifying the regulation of VRC pharmacokinetics by APS under inflammatory conditions, and providing a theoretical basis for the future prevention and treatment of drug-induced toxic effects by APS.

The detrimental effects of LPS and alcohol on the microecological system of the intestine, leading to an increased pro-inflammatory milieu in the liver, were demonstrated by Li's research group.[26,27] Using a liver inflammation model induced by the intravenous administration of small amounts of LPS, the researchers successfully demonstrated that pretreatment with probiotics enables the liver to effectively counteract the inflammation triggered by LPS-induced injury and inflammation. Consequently, an LPS-induced hepatitis model has been widely used by Chinese researchers to investigate the intricate interplay between the intestinal flora and the liver.[28,29] Previous studies by our research group illustrated that intestinal *Bacteroidetes* can effectively enhance the secretion of pro-inflammatory factors in both the intestine and liver.[5] In line with the findings of previous studies, the current study, which used the same animal model of LPS-induced inflammation, revealed a significant negative correlation between the abundance of *Bacteroidetes* and IL-1β gene expression in the environment. This study confirmed the ability of intestinal *Bacteroides* to effectively suppress the onset of inflammatory responses in the LPS-induced inflammation model. In contrast to previous research reports, this study represents the first investigation of the regulation of liver inflammatory responses by APS. Both *in vivo* and *in vitro* experiments have demonstrated that APS does not directly suppress liver inflammation, but it exerts this effect by modulating the composition of the intestinal flora. Prior research found that polysaccharides found in natural medicine can significantly influence the immune inflammatory response of the body through the gastrointestinal tract.[30] This study focused on hepatic drug metabolism, shedding light on the mechanism by which APS regulates liver drug metabolism. It has potential clinical significance for the application of APS to regulate the abnormal metabolism of voriconazole.[31]

Recent studies have illustrated the key roles of microor-

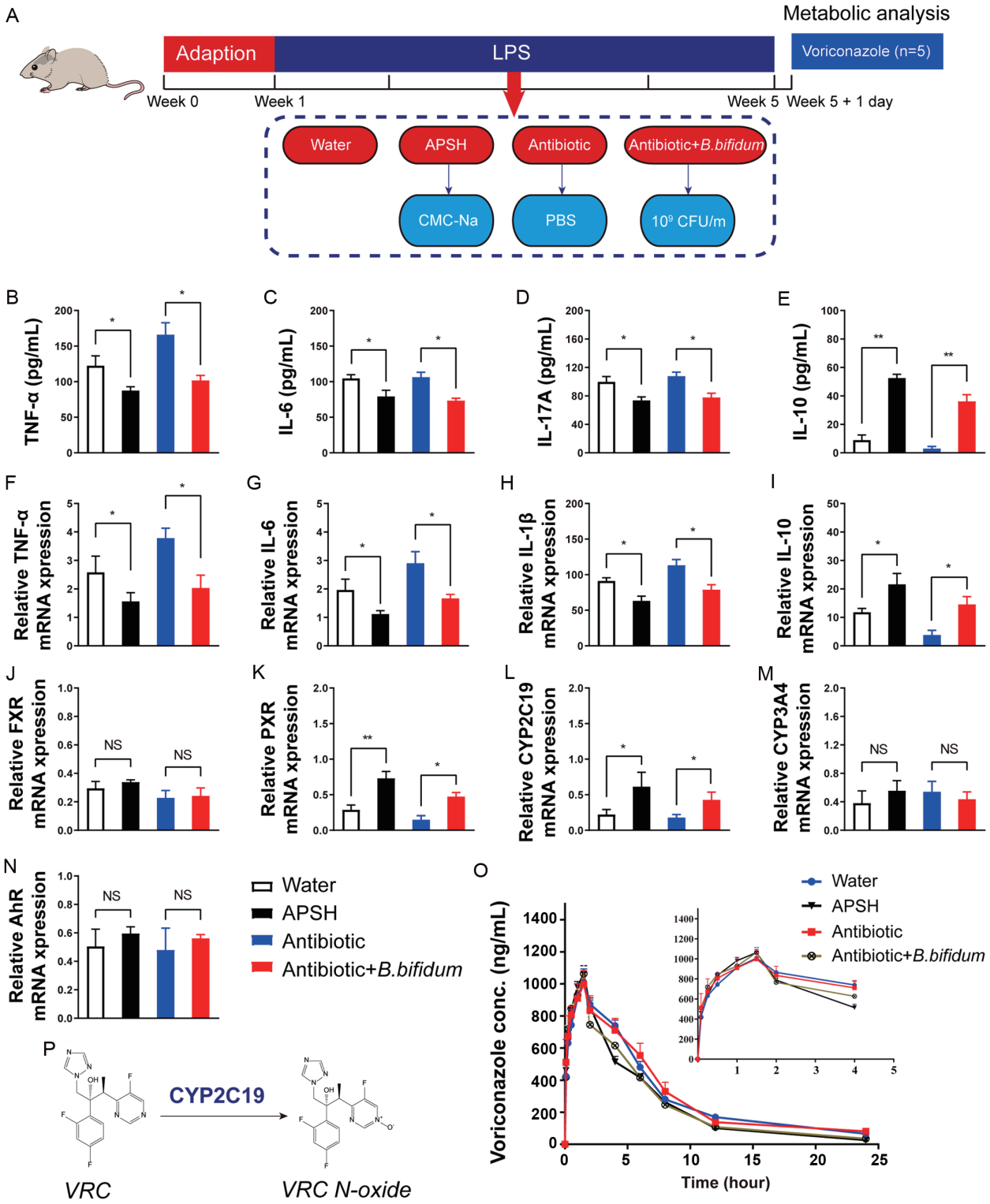

Fig. 6. *B. bifidum* inhibits liver inflammatory response and promote the metabolism of voriconazole. (A) LPS-induced inflammation model and germ-free animal working model diagram. (B–E) Quantitative analysis of inflammatory factors in each group of animals. (F–I) Analysis chart of mRNA expression of inflammatory factors in each group of animals. (J, K, N) mRNA expression analysis of nuclear transcription factors involved in drug metabolizing enzymes in hepatocytes. (L) mRNA expression analysis of CYP2C19 in hepatocytes. (M) mRNA expression analysis of CYP3A4 in hepatocytes. (O) VRC plasma kinetics in individual rats (n=5, respectively). (P) Reaction diagram of voriconazole metabolized to nitrogen oxides by CYP2C19. Data are mean±SD (n=5), $^{*}P<0.05$, $^{**}P<0.01$. AhR, Aryl hydrocarbon receptor; APSH, high-dose APS group; CMC-Na, sodium carboxymethylcellulose solution; CYP, Cytochrome P450. LPS, lipopolysaccharide; FXR, Farnesoid X receptor; IL, Interleukin; PBS, phosphate-buffered saline; PXR, pregnenolone X receptor; SD, standard deviation; TNF-α, Tumor necrosis factor; VRC, Voriconazole.

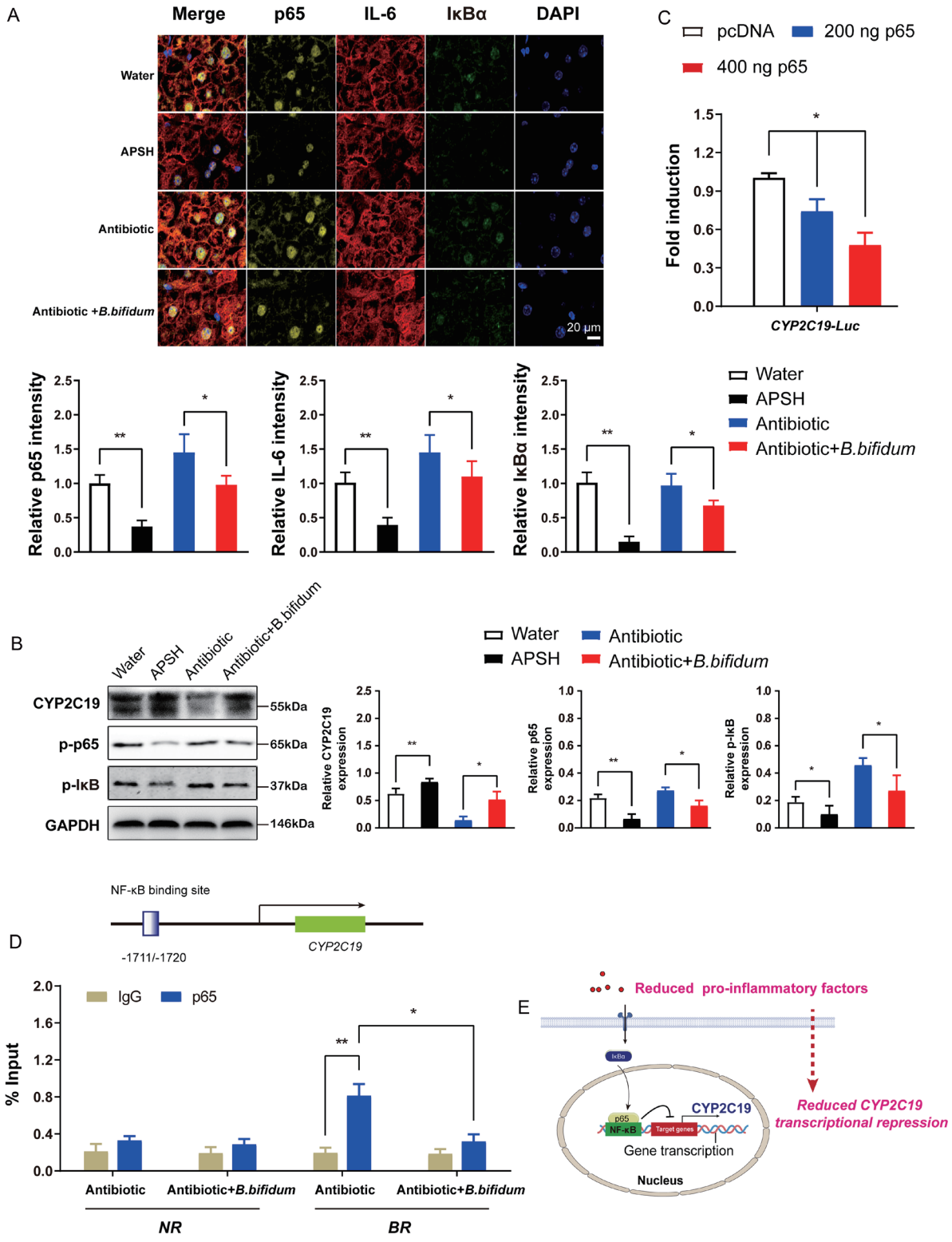

Fig. 7. Activated NF-κB in rats liver downregulates *CYP2C19* transcription. (A) Immunofluorescence expression of key proteins in the NF-κB signaling pathway of hepatocytes; (B) The indicated proteins were detected by western blot analysis. (C) Effect of p65 overexpression on CYP2C19-Luc reporter activity in hepatocytes. (D) The ChIP assays indicate that p65 is enriched near the binding site of the CYP2C19 promoter in the liver. The binding region is designated BR; the non-binding region as NR. (E) Schematic representation of the regulatory mechanism of VRC-related metabolizing enzyme CYP2C19 induced by NF-κB. Data are mean±SD (n=5), $^{*}P<0.05$, $^{**}P<0.01$ (*t*-test). APSH, high-dose APS group; B. bifidum, Bifidobacterium bifidum; CYP, Cytochrome P450; DAPI, 4′,6-diamidino-2-phenylindole; GAPDH, glyceraldehyde 3-phosphate dehydrogenase; Luc, Luciferase; NF-κB, Nuclear factor-κB; SD, standard deviation; SD, standard deviation.

ganisms in maintaining the local ecological balance of the intestine.[32,33] *B. bifidum* is a typical probiotic that can prevent further exacerbation of inflammatory activity.[34] *B. bifidum* can interact with human immune cells to generate functional Tregs.[35] In addition, *B. bifidum* can protect hepatocytes from the invasion of pathogens and alleviate alcoholic fatty liver disease by downregulating IL-6 and IL-1β,[36] consistent with our findings. The results of a study on the restoration of *B. bifidum* following the clearance of intestinal microecology indicated a consistent association between *B. bifidum* and APS in terms of anti-inflammatory factors. An analysis of the transcriptional regulatory genes PXR, CAR, and AhR, which are involved in the metabolism of exogenous substances, revealed that *B. bifidum* indirectly enhanced the transcriptional expression of PXR metabolic enzymes through its anti-inflammatory effects. These results are consistent with previous findings suggesting that PXR contributes to the regulation of human CYP2C19 transcriptase expression.[37]

In most cases, NF-κB acts as a transcriptional activator to drive target gene expression. However, there is accumulating evidence of the role of NF-κB in inflammation-induced transcriptional repression.[38] In this study, we observed that NF-κB can inhibit CYP2C19 transcription, indicating that the attenuation of NF-κB inhibition can appropriately increase CYP2C19 transcription. The metabolic capabilities of APSH and *B. bifidum* in sterilized animals demonstrated their ability to increase the transcriptional expression of CYP2C19 in an inflammatory disease environment by inhibiting the NF-κB signaling pathway. Different disease states have different effects on drug-metabolizing enzymes, with several metabolizing enzymes such as CYP, uridine 5′-diphosphate glucuronosyltransferase, sulfotransferase, and P-gp being involved in the drug metabolism process.[39,40] Numerous studies have demonstrated that phase I metabolic enzymes primarily contribute to VRC metabolism.[41] In one study, an assessment of efflux transporter activity (using testosterone as a marker) revealed that APS administration to rats with inflammation did not result in significant differences in VRC metabolism mediated by P-gp. Therefore, we analyzed the transcriptional mechanism of CYP2C19.

In experiments conducted using isolated hepatocytes, p65 overexpression interfered with CYP2C19 transcription.[5] Consequently, building on previous studies, this study attempted to predict the transcriptional promoter site of CYP2C19 that is affected by p65. This study both expands the current knowledge base and provides valuable insights for clinical conditions related to diseases. The analysis of mechanisms targeting drug-metabolizing enzymes can provide a solid scientific basis for individualized clinical treatment. It is hoped that the current findings will contribute to the advancement of polysaccharide preparations in traditional Chinese medicine and provide an empirical basis for modulating the functions of drug metabolism in patients with clinical conditions.

Conclusion

APS alleviates the reduction of VRC metabolism induced by LPS by inhibiting lipid accumulation and inflammatory cytokine levels in the serum and liver and improving the metabolic function of the liver. VRC metabolism was increased by increasing the abundance of *B. bifidum* in the intestine, reducing the secretion of anti-inflammatory factors in the liver, and increasing the activity of CYP2C19 (Fig. 7E). In particular, high-dose APS (600 mg/kg) more strongly improved VRC metabolism. These results provide important insights into the pharmacological mechanism of action of APS and the development of clinical preparations.

Acknowledgments

This paper is dedicated to the memory of Mr. Qinghou Zong, a distinguished national model worker, whose passing occurred on February 25, 2024.

Funding

This work was supported by the Discipline Construction Project of Guangdong Medical University (No. 4SG22009G), the Funds for PhD Researchers of Guangdong Medical University in 2021 (No. GDMUB2021021), the Dongguan science and technology commissioner project(20231800500332), the Guangdong province ordinary university characteristic innovation project(2020KTSCX341), the Guangdong Basic and Applied Basic Research Foundation (No. 2023A1515111116), the Science and Technology Special Fund Project of Guangdong Province in 2021 (No. 2021A05199), the Shenzhen Foundation of Science and Technology (Nos. JCYJ20230807151308018 and JCYJ20190814112205770), the Zhanjiang Science and Technology Project (2023B01176), Shenzhen Longhua District Science and Technology Innovation Fund Projects (Nos. 2022045, 2022051, 2022056, 2022095, 2022123, 2021105, 2021115 and 2020036) and the Research Foundation of Shenzhen Longhua District Central Hospital (No. 202203).

Conflict of interest

The authors have no conflict of interests related to this publication.

Author contributions

MY, JW and XY designed the whole research study. XW, XH, CY and CZ performed research. JZ and KHW collated the data and carried out data analyses. XW, SCT and LZ contributed to drafting the manuscript. All authors have read and approved the final submitted manuscript.

Ethical statement

All animal experimental procedures and post-treatments were approved by the Animal Ethics Committee of Nanfang Hospital (approval number: NFYY-2020-73).

Data sharing statement

The data used in support of the findings of this study are included within the article.

References

[1] Iyer KR, Revie NM, Fu C, Robbins N, Cowen LE. Treatment strategies for cryptococcal infection: challenges, advances and future outlook. Nat Rev Microbiol 2021;19(7):454–466. doi:10.1038/s41579-021-00511-0, PMID:33558691.

[2] Fisher MC, Henk DA, Briggs CJ, Brownstein JS, Madoff LC, McCraw SL, *et al*. Emerging fungal threats to animal, plant and ecosystem health. Nature 2012;484(7393):186–194. doi:10.1038/nature10947, PMID:22498624.

[3] Wang X, Zhao J, Wen T, Liao X, Luo B. Predictive Value of FMO3 Variants on Plasma Disposition and Adverse Reactions of Oral Voriconazole in Febrile Neutropenia. Pharmacology 2021;106(3-4):202–210. doi:10.1159/000510327, PMID:32998136.

[4] Maertens JA, Rahav G, Lee DG, Ponce-de-León A, Ramírez Sánchez IC, Klimko N, *et al*. Posaconazole versus voriconazole for primary treatment of invasive aspergillosis: a phase 3, randomised, controlled, non-inferiority trial. Lancet 2021;397(10273):499–509. doi:10.1016/S0140-6736(21)00219-1, PMID:33549194.

[5] Wang X, Ye C, Xun T, Mo L, Tong Y, Ni W, *et al*. Bacteroides Fragilis Polysaccharide A Ameliorates Abnormal Voriconazole Metabolism Accompanied With the Inhibition of TLR4/NF-κB Pathway. Front Pharmacol

2021;12:663325. doi:10.3389/fphar.2021.663325, PMID:33995087.
[6] Rausch CR, DiPippo AJ, Jiang Y, DiNardo CD, Kadia T, Maiti A, *et al*. Comparison of Mold Active Triazoles as Primary Antifungal Prophylaxis in Patients With Newly Diagnosed Acute Myeloid Leukemia in the Era of Molecularly Targeted Therapies. Clin Infect Dis 2022;75(9):1503–1510. doi:10.1093/cid/ciac230, PMID:35325094.
[7] Wang X, Tong Y, Xun T, Feng H, Lei Y, Li Y, *et al*. Functions, mechanisms, and therapeutic implications of noncoding RNA in acute myeloid leukemia. Fundam Res 2023. doi:10.1016/j.fmre.2023.04.012.
[8] Zhang ZW, Cong L, Peng R, Han P, Ma SR, Pan LB, *et al*. Transformation of berberine to its demethylated metabolites by the CYP51 enzyme in the gut microbiota. J Pharm Anal 2021;11(5):628–637. doi:10.1016/j.jpha.2020.10.001, PMID:34765276.
[9] Ying M, Yu Q, Zheng B, Wang H, Wang J, Chen S, *et al*. Cultured Cordyceps sinensis polysaccharides modulate intestinal mucosal immunity and gut microbiota in cyclophosphamide-treated mice. Carbohydr Polym 2020;235:115957. doi:10.1016/j.carbpol.2020.115957, PMID:32122493.
[10] Ni Y, Qian L, Siliceo SL, Long X, Nychas E, Liu Y, *et al*. Resistant starch decreases intrahepatic triglycerides in patients with NAFLD via gut microbiome alterations. Cell Metab 2023;35(9):1530–1547.e8. doi:10.1016/j.cmet.2023.08.002, PMID:37673036.
[11] Leung C, Rivera L, Furness JB, Angus PW. The role of the gut microbiota in NAFLD. Nat Rev Gastroenterol Hepatol 2016;13(7):412–425. doi:10.1038/nrgastro.2016.85, PMID:27273168.
[12] Ye H, Ma S, Qiu Z, Huang S, Deng G, Li Y, *et al*. Poria cocos polysaccharides rescue pyroptosis-driven gut vascular barrier disruption in order to alleviates non-alcoholic steatohepatitis. J Ethnopharmacol 2022;296:115457. doi:10.1016/j.jep.2022.115457, PMID:35753609.
[13] Lim SM, Park HB, Jin JO. Polysaccharide from Astragalus membranaceus promotes the activation of human peripheral blood and mouse spleen dendritic cells. Chin J Nat Med 2021;19(1):56–62. doi:10.1016/S1875-5364(21)60006-7, PMID:33516452.
[14] Li CX, Liu Y, Zhang YZ, Li JC, Lai J. Astragalus polysaccharide: a review of its immunomodulatory effect. Arch Pharm Res 2022;45(6):367–389. doi:10.1007/s12272-022-01393-3, PMID:35713852.
[15] Guo L, Bai SP, Zhao L, Wang XH. Astragalus polysaccharide injection integrated with vinorelbine and cisplatin for patients with advanced non-small cell lung cancer: effects on quality of life and survival. Med Oncol 2012;29(3):1656–1662. doi:10.1007/s12032-011-0068-9, PMID:21928106.
[16] Hsieh CH, Lin CY, Hsu CL, Fan KH, Huang SF, Liao CT, *et al*. Incorporation of Astragalus polysaccharides injection during concurrent chemoradiotherapy in advanced pharyngeal or laryngeal squamous cell carcinoma: preliminary experience of a phase II double-blind, randomized trial. J Cancer Res Clin Oncol 2020;146(1):33–41. doi:10.1007/s00432-019-03033-8, PMID:31728618.
[17] Li Y, Zheng J, Wang Y, Yang H, Cao L, Gan S, *et al*. Immuno-stimulatory activity of Astragalus polysaccharides in cyclophosphamide-induced immunosuppressed mice by regulating gut microbiota. Int J Biol Macromol 2023;242(Pt 2):124789. doi:10.1016/j.ijbiomac.2023.124789, PMID:37164141.
[18] Zhang R, Xu D, Zhang Y, Wang R, Yang N, Lou Y, *et al*. Silybin Restored CYP3A Expression through the Sirtuin 2/Nuclear Factor κ-B Pathway in Mouse Nonalcoholic Fatty Liver Disease. Drug Metab Dispos 2021;49(9):770–779. doi:10.1124/dmd.121.000438, PMID:34183378.
[19] Xun T, Lin Z, Zhan X, Song S, Mo L, Feng H, *et al*. Advanced oxidation protein products upregulate efflux transporter expression and activity through activation of the Nrf-2-mediated signaling pathway in vitro and in vivo. Eur J Pharm Sci 2020;149:105342. doi:10.1016/j.ejps.2020.105342, PMID:32315774.
[20] Kong X, Guo D, Liu S, Zhu Y, Yu C. Incidence, characteristics and risk factors for drug-induced liver injury in hospitalized patients: A matched case-control study. Br J Clin Pharmacol 2021;87(11):4304–4312. doi:10.1111/bcp.14847, PMID:33948989.
[21] Shen K, Gu Y, Wang Y, Lu Y, Ni Y, Zhong H, *et al*. Therapeutic drug monitoring and safety evaluation of voriconazole in the treatment of pulmonary fungal diseases. Ther Adv Drug Saf 2022;13:20420986221127503. doi:10.1177/20420986221127503, PMID:36225945.
[22] Hamada Y, Ueda T, Miyazaki Y, Nakajima K, Fukunaga K, Miyazaki T, *et al*. Effects of antifungal stewardship using therapeutic drug monitoring in voriconazole therapy on the prevention and control of hepatotoxicity and visual symptoms: A multicentre study conducted in Japan. Mycoses 2020;63(8):779–786. doi:10.1111/myc.13129, PMID:32510723.
[23] den Hollander JG, van Arkel C, Rijnders BJ, Lugtenburg PJ, de Marie S, Levin MD. Incidence of voriconazole hepatotoxicity during intravenous and oral treatment for invasive fungal infections. J Antimicrob Chemoth 2006;57(6):1248–1250. PMID:16556632.
[24] Cadena J, Levine DJ, Angel LF, Maxwell PR, Brady R, Sanchez JF, *et al*. Antifungal prophylaxis with voriconazole or itraconazole in lung transplant recipients: hepatotoxicity and effectiveness. Am J Transplant 2009;9(9):2085–2091. doi:10.1111/j.1600-6143.2009.02734.x, PMID:19645709.
[25] Zhou ZX, Yin XD, Zhang Y, Shao QH, Mao XY, Hu WJ, *et al*. Antifungal Drugs and Drug-Induced Liver Injury: A Real-World Study Leveraging the FDA Adverse Event Reporting System Database. Front Pharmacol 2022;13:891336. doi:10.3389/fphar.2022.891336, PMID:35571077.
[26] Albillos A, de Gottardi A, Rescigno M. The gut-liver axis in liver disease: Pathophysiological basis for therapy. J Hepatol 2020;72(3):558–577. doi:10.1016/j.jhep.2019.10.003, PMID:31622696.
[27] Jin P, Chen Y, Lv L, Yang J, Lu H, Li L. Lactobacillus fermentum ZYL0401 Attenuates Lipopolysaccharide-Induced Hepatic TNF-α Expression and Liver Injury via an IL-10- and PGE2-EP4-Dependent Mechanism. PLoS One 2015;10(5):e0126520. doi:10.1371/journal.pone.0126520, PMID:25978374.
[28] Zhang P, Zheng L, Duan Y, Gao Y, Gao H, Mao D, *et al*. Gut microbiota exaggerates triclosan-induced liver injury via gut-liver axis. J Hazard Mater 2022;421:126707. doi:10.1016/j.jhazmat.2021.126707, PMID:34315018.
[29] Xiao L, Hu L, Chu H, Chen L, Yan J, Wang W, *et al*. Retrorsine Cooperates with Gut Microbiota to Promote Hepatic Sinusoidal Obstruction Syndrome by Disrupting the Gut Barrier. J Clin Transl Hepato 2022;10(6):1086–1098. doi:10.14218/JCTH.2021.00398, PMID:36381109.
[30] Ma G, Du H, Hu Q, Yang W, Pei F, Xiao H. Health benefits of edible mushroom polysaccharides and associated gut microbiota regulation. Crit Rev Food Sci Nutr 2022;62(24):6646–6663. doi:10.1080/10408398.2021.1903385, PMID:33792430.
[31] Zhao Z, Liu PZ, Du PC, Zheng CY, Wang DW, Xu J, *et al*. Clinical Analysis of the Association Between Chinese Medicine Syndromes and Risk Factors for Hypertension. J Explor Res Pharmacol 2023;8(3):184–191. doi:10.14218/jerp.2022.00071.
[32] Yuan M, Hu X, Yao L, Chen P, Wang Z, Liu P, *et al*. Causal Relationship Between Gut Microbiota and Liver Cirrhosis: 16S rRNA Sequencing and Mendelian Randomization Analyses. J Clin Transl Hepato 2024;12(2):123–133. doi:10.14218/jcth.2023.00259, PMID:38343609.
[33] Zhao J, Zhao C, Xun T, Wang X, Wei S, Ye C, *et al*. Huang Gan Formula Alleviates Systemic Inflammation and Uremia in Adenine-Induced Chronic Kidney Disease Rats May Associate with Modification of Gut Microbiota and Colonic Microenvironment. Drug Des Devel Ther 2024;18:13–28. doi:10.2147/DDDT.S421446, PMID:38205394.
[34] Andresen V, Gschossmann J, Layer P. Heat-inactivated Bifidobacterium bifidum MIMBb75 (SYN-HI-001) in the treatment of irritable bowel syndrome: a multicentre, randomised, double-blind, placebo-controlled clinical trial. Lancet Gastroenterol Hepatol 2020;5(7):658–666. doi:10.1016/S2468-1253(20)30056-X, PMID:32277872.
[35] Verma R, Lee C, Jeun EJ, Yi J, Kim KS, Ghosh A, *et al*. Cell surface polysaccharides of Bifidobacterium bifidum induce the generation of Foxp3+ regulatory T cells. Sci Immunol 2018;3(28):eaat6975. doi:10.1126/sciimmunol.aat6975, PMID:30341145.
[36] Wang W, Xu AL, Li ZC, Li Y, Xu SF, Sang HC, *et al*. Combination of Probiotics and Salvia miltiorrhiza Polysaccharide Alleviates Hepatic Steatosis via Gut Microbiota Modulation and Insulin Resistance Improvement in High Fat-Induced NAFLD Mice. Diabetes Metab J 2020;44(2):336–348. doi:10.4093/dmj.2019.0042, PMID:31950772.
[37] Shu W, Guan S, Yang X, Liang L, Li J, Chen Z, *et al*. Genetic markers in CYP2C19 and CYP2B6 for prediction of cyclophosphamide's 4-hydroxylation, efficacy and side effects in Chinese patients with systemic lupus erythematosus. Br J Clin Pharmacol 2016;81(2):327–340. doi:10.1111/bcp.12800, PMID:26456622.
[38] Ma L, Zeng W, Tan Z, Wang R, Yang Y, Lin S, *et al*. Activated Hepatic Nuclear Factor-κB in Experimental Colitis Regulates CYP2A5 and Metronidazole Disposition. Mol Pharm 2023;20(2):1222–1229. doi:10.1021/acs.molpharmaceut.2c00890, PMID:36583631.
[39] Stingl JC, Bartels H, Viviani R, Lehmann ML, Brockmöller J. Relevance of UDP-glucuronosyltransferase polymorphisms for drug dosing: A quantitative systematic review. Pharmacol Therapeut 2014;141(1):92–116. doi:10.1016/j.pharmthera.2013.09.002, PMID:24076267.
[40] Collins SL, Patterson AD. The gut microbiome: an orchestrator of xenobiotic metabolism. Acta Pharm Sin B 2020;10(1):19–32. doi:10.1016/j.apsb.2019.12.001, PMID:31998605.
[41] Zhao Y, Chen P, Dou L, Li F, Li M, Xu L, *et al*. Co-Administration with Voriconazole Doubles the Exposure of Ruxolitinib in Patients with Hematological Malignancies. Drug Des Devel Ther 2022;16:817–825. doi:10.2147/DDDT.S354270, PMID:35370398.